AGU PUBLICATIONS

Geophysical Research Letters

RESEARCH LETTER
10.1002/2017GL076486

Key Points:
- A theoretically expected 1 Hz luminous modulation of proton aurora was detected
- The 1 Hz luminous modulation showed a high correlation with Pc1 wave power
- The inferred IPA source regions for the 1 Hz modulation were distributed around the magnetic equator

Supporting Information:
- Supporting Information S1
- Movie S1
- Movie S2

Correspondence to:
M. Ozaki,
ozaki@is.t.kanazawa-u.ac.jp

Citation:
Ozaki, M., Shiokawa, K., Miyoshi, Y., Kataoka, R., Connors, M., Inoue, T., … Danskin, D. W. (2018). Discovery of 1 Hz range modulation of isolated proton aurora at subauroral latitudes. *Geophysical Research Letters*, *45*, 1209–1217. https://doi.org/10.1002/2017GL076486

Received 22 NOV 2017
Accepted 29 DEC 2017
Accepted article online 4 JAN 2018
Published online 5 FEB 2018

©2018. The Authors.
This is an open access article under the terms of the Creative Commons Attribution-NonCommercial-NoDerivs License, which permits use and distribution in any medium, provided the original work is properly cited, the use is non-commercial and no modifications or adaptations are made.

Discovery of 1 Hz Range Modulation of Isolated Proton Aurora at Subauroral Latitudes

M. Ozaki[1], K. Shiokawa[2], Y. Miyoshi[2], R. Kataoka[3,4], M. Connors[5], T. Inoue[1], S. Yagitani[1], Y. Ebihara[6], C.-W. Jun[7], R. Nomura[8], K. Sakaguchi[9], Y. Otsuka[2], H. A. Uchida[4], I. Schofield[5], and D. W. Danskin[10]

[1]Graduate School of Natural Science and Technology, Kanazawa University, Kanazawa, Japan, [2]Institute for Space-Earth Environmental Research, Nagoya University, Nagoya, Japan, [3]National Institute of Polar Research, Tachikawa, Japan, [4]Department of Polar Science, Graduate University for Advanced Studies (SOKENDAI), Tachikawa, Japan, [5]Center for Science, Athabasca University, Athabasca, Alberta, Canada, [6]Research Institute for Sustainable Humanosphere, Kyoto University, Uji, Japan, [7]Department of Atmospheric and Oceanic Sciences, University of California, Los Angeles, CA, USA, [8]Japan Aerospace Exploration Agency, Tsukuba, Japan, [9]National Institute of Information and Communications Technology, Koganei, Japan, [10]Natural Resources Canada, Ottawa, Ontario, Canada

Abstract Isolated proton aurora (IPA) is a manifestation of the wave-particle interaction visible at subauroral latitudes, with activity on many timescales. We herein present the first observational evidence of rapid luminous modulation of IPA correlated with simultaneously observed Pc1 waves observed on the ground, which are equivalent to the electromagnetic ion cyclotron (EMIC) waves in the magnetosphere. The fastest luminous modulation of IPA was observed in the 1 Hz frequency range, which was twice the frequency of the related Pc1 waves. The time lag between variations of Pc1 wave power and the IPA luminosity suggests that the source regions of IPA are distributed near the magnetic equator, suggesting an EMIC wave-energetic (a few tens of keV) proton or relativistic (MeV or sub-MeV) electron interaction. The generation mechanism of this 1 Hz luminous modulation remains an open issue, but this study supports the importance of nonlinear pitch angle scattering via wave-particle interactions.

Plain Language Summary This study presents the discovery of a direct link between isolated proton aurora and natural electromagnetic waves known as electromagnetic ion cyclotron (EMIC) waves detected as Pc1 geomagnetic pulsations on the ground. For the first time, the fastest expected variations are detected through fast modulations of isolated proton aurora. The isolated proton aurora comes from the Earth's radiation belts, driven by plasma waves via wave-particle interaction. Theoretical studies have shown that the isolated proton aurora is generated by resonant interaction with EMIC waves. Our finding gives a clear observational evidence of this by using cutting edge observations, related to this essential physical process for energy transport in plasmas.

1. Introduction

Isolated proton aurora (IPA) allows the diagnosis of localized wave-particle interaction in the inner magnetosphere. Recently, pulsating IPA was discovered at subauroral latitudes (Nomura et al., 2016; Ozaki et al., 2016). The likely IPA generation mechanism is pitch angle scattering of protons by electromagnetic ion cyclotron (EMIC) waves undergoing wave-particle interactions at the magnetic equator (e.g., Albert, 2003; Jordanova et al., 2001; Kennel & Petschek, 1966; Shoji & Omura, 2014), which leads to proton precipitation in the energy range from 30 to 800 keV (Hyun et al., 2014; Yahnin et al., 2007). Previous studies supported this idea through simultaneous observations of IPA and related EMIC/Pc1 (0.2 to 5 s periods) waves (Miyoshi et al., 2008; Sakaguchi et al., 2007, 2008, 2012). EMIC/Pc1 waves play an important role not only in the removal of protons from the ring current but also in rapid removal of relativistic electrons from the radiation belts (Clilverd et al., 2015; Hendry et al., 2017; Miyoshi et al., 2008; Rodger et al., 2008; Usanova et al., 2010, 2014). A coordinated ground and Van Allen Probes observation showed that structured Pc1 waves in the magnetosphere can propagate to the ground without significant frequency dispersion (Paulson et al., 2014). The Pc1 waves on the ground can be equivalent to the EMIC waves in the magnetosphere. To date, three temporal characteristics of EMIC/Pc1 waves have been observed. First, the duration of a bundle of EMIC/Pc1 waves is several tens of minutes to several hours. Second, EMIC/Pc1 waves show successive discrete elements, known as pearl structures, in the range of several tens of seconds to a few minutes. Third, the discrete element of EMIC/Pc1 waves

includes subpacket structures that appear as nonperiodic amplitude modulations on the timescale of a few tens of seconds. In accordance with the temporal characteristics of EMIC/Pc1 waves, a statistical link between the occurrence of IPA and Pc1 waves has been reported based on several ground-based and satellite observations (Sakaguchi et al., 2008; Usanova et al., 2010; Yahnin et al., 2007). The duration of events (minutes to several hours), luminous intervals (a few minutes), and luminous modulation (a few tens of seconds), have all been found in IPA by using the most advanced (Electron Multiplying Charge Coupled Device (EMCCD)) cameras (Ozaki et al., 2016). Theoretical studies support the various timescales mentioned above (Kubota et al., 2015; Shoji & Omura, 2014) and also suggest that faster variations at a frequency of approximately 1 Hz should exist. Since proton auroras are faint (Eather, 1967), direct detection of fast visible light fluctuations is difficult, even with EMCCD cameras. Advanced analysis in the time-frequency domain must be applied to images from the most sensitive EMCCD cameras to reveal this never-before-seen fast flickering of IPA.

Here we report that a high-frequency (approximately 1 Hz) signal is present in IPA luminous variations, at twice the associated Pc1 wave frequency, constituting the predicted rapid flickering of IPA. This is the first observational evidence of the direct association of rapid luminous variations of IPA with individual cycles of Pc1 waves.

2. Observations

Two events showing the fastest luminous modulations of IPA and associated Pc1 waves detected by the ground-based induction magnetometer (Shiokawa et al., 2010) (see Text S1 in the supporting information) were observed at Athabasca on the duskside (ATH, 54.7 N, 246.7°E, L = 4.5) (see Table S1). The IPA was observed with no contamination from the more poleward electron auroras (see Figure S1 and Movies S1 and S2). The IPA were recorded by all-sky EMCCD cameras (see Text S2). A BG3 glass filter was used to suppress the long-lived green (555.7 nm) and red (630.0 nm) emissions for the high-speed EMCCD camera (Samara et al., 2012; Semeter et al., 2008). Sounding rocket and satellite experiments have spatial and temporal limitations and ambiguity in matching other data sets, as well as a limited data capacity. These are overcome by ground-based observations, which allow continuous monitoring of IPA with a better spatial coverage (approximately 1,000 km) and a high time resolution (1/8 s). This enables comparison between high-speed IPA images and the generation frequencies of related Pc1 waves.

Figure 1 shows a selected event with simultaneous ground-based observations of pulsating IPA and related Pc1 waves at ATH on 2 January 2016. A clear IPA was observed near the zenith of ATH during the geomagnetic field disturbance in a late recovery phase of a geomagnetic storm (*Dst* index = −25 nT), as shown in Figure 1a. The dynamic spectrum of the Pc1 waves (Figure 1d) was calculated from the short-time Fourier transform (STFT). The related Pc1 waves exhibit rising and falling tone elements in the He+ band between He+ and O+ equatorial cyclotron frequencies (1.5 Hz and 0.38 Hz, respectively) calculated using the Tsyganenko model (Tsyganenko, 2002a, 2002b). Such rising and falling tone structures of EMIC waves are important in nonlinear wave growth (Shoji & Omura, 2013, 2017). The spectral characteristics are somewhat different from those expected from nonlinear-triggered emissions as modeled by Shoji and Omura (2013, 2017). We will carefully investigate the difference in the future. The center frequency of the Pc1 waves is approximately 0.6 Hz. The BG3 images are wideband but are colocated with Hbeta (Hydrogen Balmer ®, wavelength of 486.1 nm) emissions, which are a signature of energetic (several tens of keV) proton precipitation. The other IPA event on 12 November 2015 is the same as that presented in Ozaki et al. (2016). Both pulsating IPA events are highly correlated with the Pc1 intensity variations, which are calculated as the integration from 0.35 to 0.90 Hz in Figure 1d. The correlation value between the Pc1 and BG3 intensities exceeds 0.75. Although the Pc1 waves can be trapped in the ionospheric duct and horizontally propagate over a long distance (1,000 km) (Kim et al., 2010), this high correlation above the observation site supports the hypothesis that the observed Pc1 waves penetrate an ionospheric exit point and reach the ground station without the horizontal propagation in the ionospheric duct. Furthermore, the association with Hbeta supports the basic idea that the high-energy protons responsible for the generation of pulsating IPA originate from resonant interaction with Pc1 waves. Since it is difficult to identify the fastest temporal variations of IPA in the time domain alone, we used the Stockwell transform (Stockwell et al., 1996) to perform time-frequency analysis. One of the advantages of the Stockwell transform is that it has a frequency-dependent resolution in the

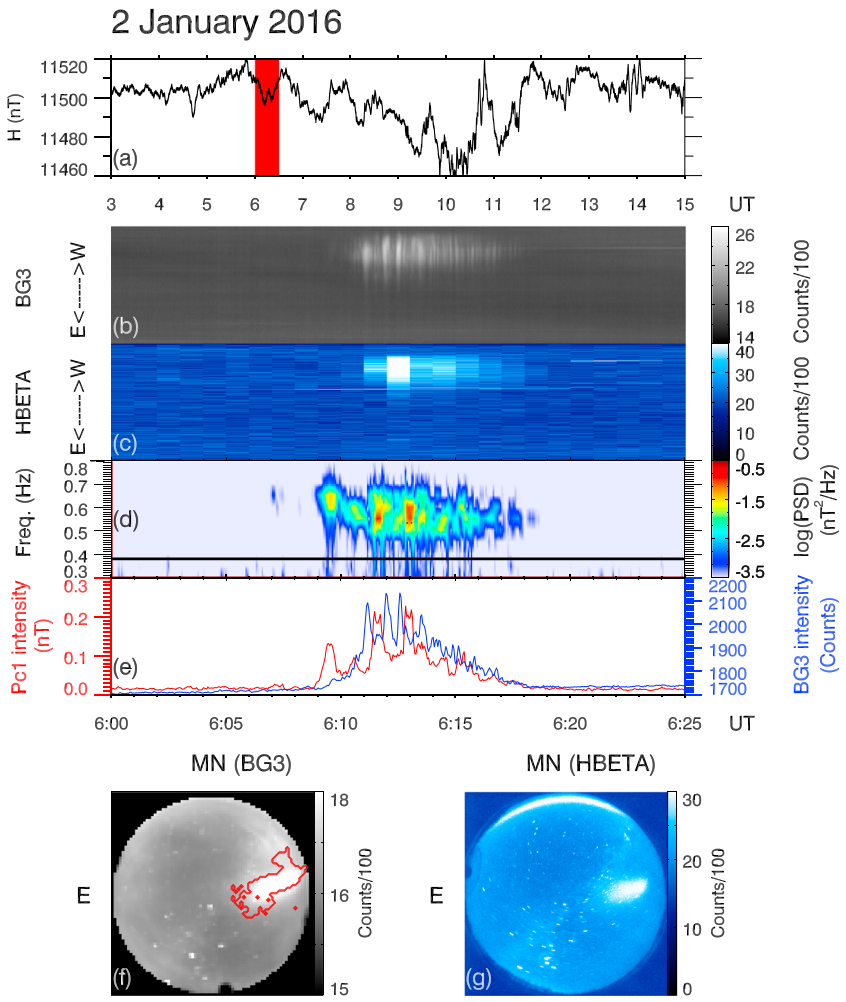

Figure 1. Selected IPA event on 2 January 2016. (a) Earth's magnetic field data at ATH for the north component. The red rectangle indicates the IPA event. (b and c) East-west ewograms for the BG3 and Hbeta all-sky images. (d) Dynamic spectrum of the Pc1 waves. The black line indicates the O+ cyclotron frequency (0.38 Hz) at the magnetic equator. (e) Pc1 intensity (integration from 0.35 to 0.90 Hz) and BG3 intensity in the proton spot. (f and g) Averaged BG3 and Hbeta images, with magnetic north (MN) at the top. The red outline denotes the proton spot that is highly correlated with the Pc1 intensity (greater than 0.75).

time-frequency analysis. On the other hand, the STFT has a fixed frequency resolution due to a constant time window width. Therefore, the Stockwell transform allows a better detection of a higher-frequency burst and yields a better signal clarity than the STFT.

Figures 2a and 2b show the frequency-time diagrams of the averaged BG3 intensity in the proton spot and the squared amplitude of the magnetic field for the geomagnetic north component using the Stockwell transform. The squared amplitude of the magnetic field is proportional to the Pc1 wave power. Figures 2c and 2d show the other IPA event calculated in the same manner as for Figures 2a and 2b. The magnified diagrams in the frequency range from 0.5 Hz to 2.0 are shown in Figures S2 and S3. In addition, the luminous intensity maps for each frequency (see Text S3) are shown in Figures S4 and S5. If the time variation is as $\exp(j\omega t)$ for the electromagnetic fields of the Pc1 waves, where j is the imaginary unit, ω is the angular frequency, and t is the time, then the wave power is proportional to $\exp(j2\omega t)$. Thus, the 1 Hz range fluctuations in Figures 2b and 2d reflect the fluctuations of wave power of the Pc1 waves at the center frequency of 0.6 Hz shown in Figure 1d. Here we refer to fluctuations related to the Pc1 pearl structure, the subpacket structure, and the wave power as the main, fast, and 1 Hz modulations, respectively. There is a strong association between the Pc1 wave power and the 1 Hz IPA modulations seen in Figures 2a and 2c. The 1 Hz IPA

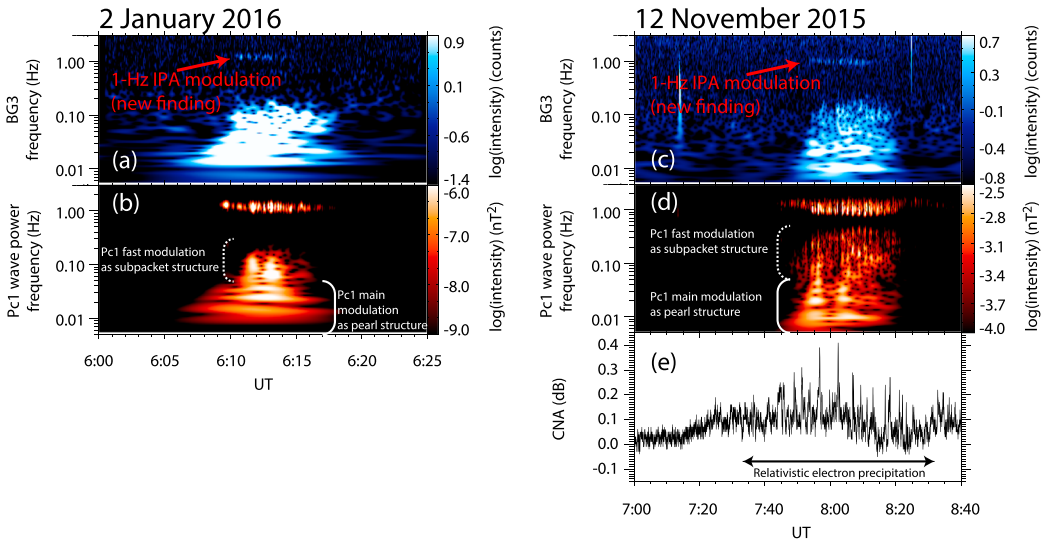

Figure 2. Frequency-time diagrams of (a and c) the IPA luminosity and (b and d) the squared amplitude of magnetic field for the geomagnetic north component. (e) CNA variations during the IPA event on 12 November 2015.

modulation occurred intermittently with frequency-time characteristics similar to those of the Pc1 wave power. Furthermore, in the IPA event on 12 November 2015, as shown in Figure 2e, a cosmic noise absorption (CNA) was simultaneously observed at Meanook (54.6 N, 246.7°E) (see Text S4), which is approximately 20 km east from ATH. The CNA levels reached 0.4 dB with a pulse width of 20 s during the pulsating IPA event. The CNA variations are a signature of intermittent relativistic (MeV or sub-MeV) electron precipitation into the IPA from the radiation belts (Clilverd et al., 2015; Rodger et al., 2008). Unfortunately, the CNA on 2 January 2016 (not shown herein) did not exhibit such spiky variations, due to contamination by artificial noises.

3. Estimation of the Source Region

There are two possible explanations for the generation region of the observed 1 Hz luminosity modulations. One is the auroral acceleration region near the Earth at altitudes of 1 to 2 times the Earth's radius. The generation region of the 1 Hz modulation could be near the auroral acceleration regions in the ionospheric Alfven resonator (Chaston et al., 2002; Fukuda et al., 2017; Lysak & Song, 2005). Although the spectrum harmonics of the magnetic field usually associated with the ionospheric Alfven resonance (IAR) were observed until 05 UT on 12 November 2015, clear IAR events were not observed during either IPA event. Another source could be in the magnetosphere far from auroral acceleration regions, such as the magnetic equator. Figures 3a and 3b show the cross-correlation values between the Pc1 wave power and the IPA luminosity for each modulation. Here it is assumed that the main and fast modulations are in the frequency ranges of 0.005 Hz to 0.050 Hz and 0.050 Hz to 0.500 Hz, respectively, and that the frequency ranges of 1 Hz modulation are 1.000 to 1.400 Hz for the event on 2 January 2016 and 0.500 Hz to 1.500 Hz for the event on 12 November 2015. The Pc1 wave power and IPA luminosity for each modulation are calculated from the convolution integral with the band-pass filter for each modulation, and the cross-correlation analysis was then performed using the filtered Pc1 wave power and the filtered IPA luminosity for each modulation (see Text S5). Clear peaks of time lag for the main (showing the pearl structure), fast (showing the subpacket structure), and 1 Hz (new finding in the present study) modulations were obtained. Since the correlation values depend on the time segment and the signal-to-noise ratio (SNR), the most important point is that the correlation value for the 1 Hz modulation showed a clear peak in a low-SNR situation in both events. A positive time lag indicates that particles arrived above the ground station faster than waves. The clear time lag between waves and particles indicates that the waves and particles should travel along a long field line with different velocities, which supports the hypothesis that the source region is far from the auroral acceleration regions. In the event on 2 January 2016, the time lags for the main and fast modulations were approximately +40 s and

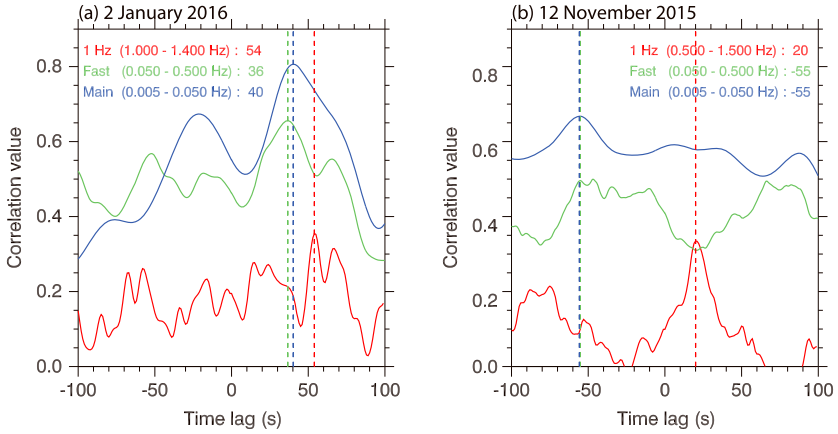

Figure 3. Correlation analysis results between the Pc1 wave power and the IPA luminosity for the events on (a) 2 January 2016 and (b) 12 November 2015 as a function of time lag. The blue, green, and red curves indicate the correlation values for the main, fast, and 1 Hz modulations, respectively.

the 1 Hz modulation had a peak at +54 s. These results indicate that the precipitating particles related to all (main, fast, and 1 Hz ranges) of the modulations traveled to the ground faster than the Pc1 waves. In the event on 12 November 2015, the time lags for the main and fast modulations were the same value of −55 s and that for the 1 Hz modulation was +20 s. Note that the time lags for the fast modulation were approximately the same as those for the main modulation in both events, which suggests that the source regions for the main and fast modulations of IPA are the same in the magnetosphere. Furthermore, the time lag for the 1 Hz modulation took a positive value in both events. The particle energy related to the 1 Hz IPA modulation can be very high in comparison with that for the main and fast modulations, because the precipitation particles related to the 1 Hz IPA modulation reached the ground faster than the waves, regardless of the time lags for the main and fast modulations.

In order to identify the source regions of the IPA, the interaction regions between EMIC/Pc1 waves and energetic particles are estimated from the difference in their travel times. In the present study, we estimate the source regions of the IPA based on Mende et al. (1980). The time difference between the EMIC waves and the energetic particles is calculated theoretically. In the theoretical calculation, the EMIC waves and energetic particles are assumed to travel along the same magnetic field line. In order to simplify the estimation, the effects of the oblique propagation and ion composition ratio on the EMIC waves are not considered in the present study. The group velocity $v_g(s)$ of parallel propagation of the EMIC wave along a field line is written as (Kennel & Petschek, 1966)

$$v_g(s) = V_A(s)\left(1-\frac{\omega}{\omega_{ci}(s)}\right)^{\frac{3}{2}}\left(1-\frac{\omega}{2\omega_{ci}(s)}\right)^{-1}, \quad (1)$$

where ω_{ci} is the cyclotron angular frequency of proton, s is location along the field line, and $V_A = B/(\mu_0 N m_H)^{1/2}$ is the Alfven velocity defined by the magnetic field B, the permeability in vacuum μ_0, the number density N, and the proton mass m_H. The parallel velocity of energetic protons is

$$v_{\parallel}(s) = \left\{\left(\frac{2E_L}{m_H}\right)\left(1-\sin^2\alpha\frac{B(s)}{B(s_i)}\right)\right\}^{\frac{1}{2}}, \quad (2)$$

where E_L is the kinetic energy and α is the loss cone at a possible source location s_i. The parallel velocity of a relativistic electron within the loss cone is

$$v_{\parallel}(s) = \frac{p_e}{m_e\gamma_e}\cos\alpha, \quad (3)$$

where p_e, m_e, and γ_e are the momentum, electron mass, and relativistic Lorentz gamma, respectively (Saito et al., 2012). The number density N along the field line is computed from the plasmaspheric model under the hydrostatic assumption (Miyoshi et al., 2006; Rasmussen et al., 1993). The values of the number density at the equator were 52.7 particles/cm^3 for the event on 2 January 2016 and 111 particles/cm^3 for the

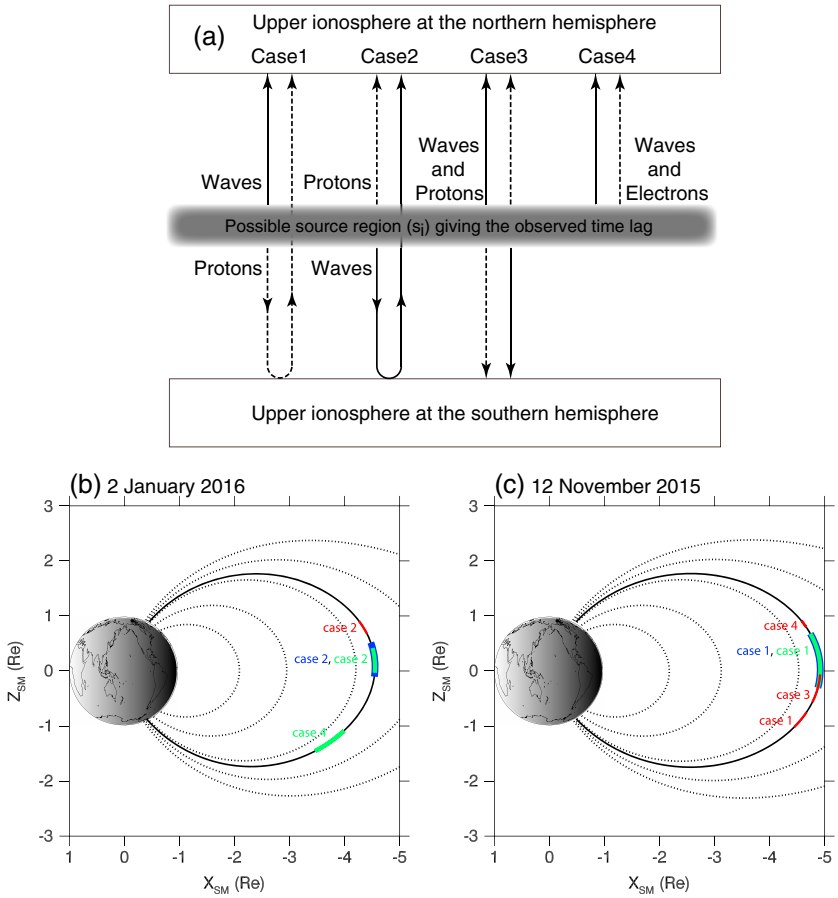

Figure 4. (a) Four possible wave-particle interaction cases that could yield the observed time lag. (b and c) Estimated source regions for the main (blue), fast (green), and 1 Hz (red) modulations.

event on 12 November 2015. The magnetic field B is calculated from the Tsyganenko model (Tsyganenko, 2002a, 2002b). As shown in Figure 4a, four possible wave-particle interaction cases that could yield the observed time lag are considered. Cases 1 to 3 involve possible cyclotron resonance conditions between EMIC waves and protons. The parallel energy of protons in cases 1 to 3 is given by the cyclotron resonance condition at wave-particle interaction location s_i as (Kennel & Petschek, 1966)

$$E_L = \frac{B^2(s_i)}{2\mu_0 N(s_i)} \left(\frac{\omega_{ci}(s_i)}{\omega}\right)^2 \left(1 - \frac{\omega}{\omega_{ci}(s_i)}\right)^3. \quad (4)$$

The resonant energy of protons increases with latitude, and their maximum resonant energy is probably approximately 100 keV (Miyoshi et al., 2008). Since the trapped protons with energy on the order of 10 keV dominate between L = 4 and 9 (Milillo et al., 2001), the EMIC waves most likely resonate with the trapped protons. Thus, the maximum proton energy in the estimated source region is assumed to be up to 100 keV. Case 4 is a possible resonance condition between EMIC waves and relativistic (MeV or sub-MeV) electrons at possible source location s_i. Relativistic electrons over 1 MeV can interact with EMIC waves (Kubota et al., 2015; Miyoshi et al., 2008; Omura & Zhao, 2013), but such higher energy electrons cannot contribute to auroral emissions. The electron resonance energy in the estimation of the source region is assumed to be from 500 keV to 1 MeV. The theoretical time difference between EMIC waves and energetic particles is calculated for each case. Then, the wave-particle interaction region is determined as the location at which the theoretical time difference corresponds to the observed time lag (Figure 3).

Figures 4b and 4c show the estimated source regions in solar magnetic coordinates. The black (solid for ATH and dotted for reference) curves show the magnetic field lines calculated from the Tsyganenko model. The estimated source regions for both IPA events are mostly concentrated around the magnetic equator,

except for the source region of the fast modulation for the event on 2 January 2016 given by case 4. Since the time lags for the main and fast modulations were approximately the same in both events, their estimated source regions were located in the same regions near the equator as a result of case 2 for the event on 2 January 2016 and as a result of case 1 for the event on 12 November 2015. The source regions of all modulations on 2 January 2016 were given by case 2, which indicates the situation in which scattered protons reach the ground station, followed by waves reflected at the opposite hemisphere. The resonant energy ranges of protons in the estimated source regions for the main, fast, and 1 Hz modulations are 17 to 48 keV, 14 to 28 keV, and 47 to 83 keV, respectively, which interact with EMIC waves in the frequency range of 0.5 to 0.8 Hz. Moreover, the source region of the fast modulation was given as resulting from case 4. The EMIC wave-relativistic electron interaction region given by case 4 was located at higher latitudes in comparison with the EMIC wave-energetic proton interaction regions given by case 2. Next, the source regions of all modulations on 12 November 2015 were given as resulting from case 1, indicating that EMIC waves reach the ground, followed by energetic protons reflected at the opposite hemisphere. The resonant energy range of protons in the source regions for the main, fast, and 1 Hz modulations are 6 to 11 keV, 6 to 11 keV, and 48 to 96 keV, respectively, which interact with EMIC waves in the frequency range of 0.4 to 0.8 Hz. The other source regions for the 1 Hz modulation were given by cases 3 and 4. The energy range of the 1 Hz modulation given by case 3 was 10 to 34 keV. The possible source regions of the 1 Hz modulation were distributed near the equator within the magnetic latitude from −14 to +11° in both events, as a result of the EMIC wave-energetic proton interaction for the event on 2 January 2016 and as a result of the EMIC wave-relativistic electron interaction for the event on 12 November 2015. The source regions of the 1 Hz modulation exhibited mostly higher latitudes and higher resonant proton energies than for the main and fast modulations.

The calculation examples of the theoretical time difference are plotted in Figures S6 and S7. The estimation results include the ambiguities of plasma density and geomagnetic field caused by their model accuracies, but these parameters affect both the wave and particle velocities, as expressed by equations (1) to (4). The ambiguities of plasma density and geomagnetic field do not have a major effect on the estimation of the source region, even if the plasma density includes errors of −10% to +50%. Moreover, even if there is a reflection boundary up to the altitude of 10,000 km by the effect of bi-ion frequency (Thorne & Horne, 1993), the estimated source regions are still concentrated in the equatorial regions. This is because the travel time of waves and the particle velocity around the equator are dominant, as shown in Figures S6 and S7. However, future studies are needed in order to estimate the source regions using more realistic models. In future studies, we will take into account the effects of the oblique propagation and the ion composition ratio on the EMIC waves.

4. Discussion

The Combined Release and Radiation Effects Satellite (CRRES) observations in the inner magnetosphere showed that the source regions of EMIC waves were distributed within 11° of the magnetic equator (Loto'aniu et al., 2005), but the Earth's magnetic field was approximated as a simple dipole field. Shoji and Omura (2013) suggested that the subpacket structures of EMIC waves are formed by a superposition of EMIC waves repeatedly and nonlinearly triggered near the equator. Kubota et al. (2015) showed that the EMIC waves having subpacket structures more effectively interact with relativistic electrons. Our estimation results showed that the source regions for the main and fast modulations were distributed near the equator, resulting in EMIC wave-energetic proton/relativistic electron interactions. The estimation results support the above mentioned observation and simulation studies. The results of a recent computer simulation study suggest a modulation of a few seconds of precipitating particles scattered at the magnetic equator due to a nonlinear effect (Shoji & Omura, 2014). Moreover, our estimation results showed the existence of the source regions of 1 Hz luminous modulation resulting from EMIC wave-energetic proton interactions (cases 1 to 3). On the other hand, Kataoka et al. (2016) showed that 5 to 20 s modulations of relativistic electron precipitation (REP) around the boundary of the plasmapause regularly exist based on measurements by a charge detector on board the international space station (ISS). The observed 1 Hz modulation is 5 to 20 times faster than such modulations during REP events observed at the ISS. The travel time of MeV or sub-MeV electrons is incomparably faster than that for the EMIC waves and the 1–100 keV protons. The time-of-flight (TOF) effect for a wide energy range of REP would be negligible in comparison with the TOF effect for precipitating protons, because the velocity approaches the speed of light. In order to support the REP during the IPA event,

the spiky CNA was simultaneously observed at Meanook near ATH, as shown in Figure 2e. The estimated source region of 1 Hz luminous modulation for the event on 12 November 2015 is distributed near the equator as a result of EMIC wave-relativistic electron interactions (case 4). Based on these observations and estimations of the source regions, MeV and sub-MeV electrons can cause an electron aurora simultaneously with the IPA. Marshall et al. (2014) simulated optical emissions generated by relativistic electron beam using a Monte Carlo model. The dominant emissions are the first and second positive systems of N_2 and the first negative systems of N_2^+ in their simulations. Therefore, we consider that the fast-oscillating auroral emissions observed by the BG3 filter (transmission wavelengths at 300–500 nm and above 700 nm) are caused at the N_2 first (~700–900 nm) and second (300–400 nm) positive bands and the N_2^+ first negative band (320–500 nm).

5. Conclusions

Ground-based observations of luminous variations of IPA provide clear experimental evidence that the origin of the IPA is the resonant interaction with Pc1/EMIC waves on various timescales (1 s to a few tens of minutes). Never-before-seen temporal characteristics of the IPA were observed based on high-speed EMCCD images with the Stockwell transform. Although the detailed generation mechanism of the 1 Hz IPA modulation remains an open issue, the nonlinear pitch angle scattering process by EMIC waves is a major candidate. The key findings of the present study are as follows:

1. The 1 Hz IPA modulation has a remarkable correlation with the Pc1 wave power (cf. Figure 2).
2. The frequency of the 1 Hz IPA modulation is twice that of the Pc1 wave (cf. Figure 2).
3. The CNA burst, which is indirect evidence of REP, was simultaneously observed during the pulsating IPA event on 12 November 2015.
4. The precipitating particles related to the 1 Hz IPA modulation reached the ground faster than the waves. Thus, the particle energy should be very high (cf. Figure 3).
5. The source regions of the main and fast modulations were concentrated around the equator (cf. Figure 4).
6. The source regions of the 1 Hz IPA modulation were also given near the equator as resulting from the EMIC wave-energetic proton or relativistic (MeV or sub-MeV) electron interaction (cf. Figure 4).

These findings provide a new framework for understanding the complicated dynamics of coupling of waves and particles in the radiation belts. In the future, comparison between ground (wave and aurora) and satellite (wave and particle) observations will be important for estimating the detailed resonance energy in the 1 Hz IPA event.

Acknowledgments
The present study was supported by JSPS KAKENHI grants 15H05747, 15H05815, 16H06286, and 17K06456 and by the Kanazawa University SAKIGAKE project. This study was also supported by JSPS Bilateral Open Partnership Joint Research Projects. The observations at the Athabasca University Geospace Observatory were supported by the Canada Foundation for Innovation. The authors would like to thank Y. Kato, Y. Hamaguchi, Y. Yamamoto, and T. Adachi of ISEE, Nagoya University, and K. Reiter of Athabasca University Geospace Observatory for their helpful support in the operation of the induction magnetometer and optical observations. M. C. acknowledges support as Visiting Foreign Professor at Nagoya University during this project. The induction magnetometer data at ATH were obtained from http://stdb2.stelab.nagoya-u.ac.jp/magne/index.html. The all-sky EMCCD data captured with a BG3 glass filter at ATH are available through ERG-Science Center, ISEE, Nagoya University. The all-sky EMCCD data for Hbeta emissions and the magnetometer data at ATH were obtained from http://autumn.athabascau.ca. The broad-beam CNA data at Meanook are available through Natural Resources Canada. The *Kp* and *Dst* indices were provided by the WDC for Geomagnetism in Kyoto (http://wdc.kugi.kyoto-u.ac.jp/).

References

Albert, J. M. (2003). Evaluation of quasi-linear diffusion coefficients for EMIC waves in a multispecies plasma. *Journal of Geophysical Research*, *108*(A6), 1249. https://doi.org/10.1029/2002JA009792

Chaston, C. C., Bonnell, J. W., Carlson, C. W., Berthomier, M., Peticolas, L. M., Roth, I., … Strangeway, R. J. (2002). Electron acceleration in the ionospheric Alfven resonator. *Journal of Geophysical Research*, *107*(A11), 1413. https://doi.org/10.1029/2002JA009272

Clilverd, M. A., Duthie, R., Hardman, R., Hendry, A. T., Rodger, C. J., Raita, T., … Milling, D. K. (2015). Electron precipitation from EMIC waves: A case study from 31 May 2013. *Journal of Geophysical Research: Space Physics*, *120*, 3618–3631. https://doi.org/10.1002/2015JA021090

Eather, R. H. (1967). Auroral proton precipitation and hydrogen emissions. *Reviews of Geophysics*, *5*, 207–285. https://doi.org/10.1029/RG005i003p00207

Fukuda, Y., Kataoka, R., Uchida, H. A., Miyoshi, Y., Hampton, D., Shiokawa, K., … Seki, K. (2017). First evidence of patchy flickering aurora modulated by multi-ion electromagnetic ion cyclotron waves. *Geophysical Research Letters*, *44*, 3963–3970. https://doi.org/10.1002/2017GL072956

Hendry, A. T., Rodger, C. J., & Clilverd, M. A. (2017). Evidence of sub-MeV EMIC-driven electron precipitation. *Geophysical Research Letters*, *44*, 1210–1218. https://doi.org/10.1002/2016GL071807

Hyun, K., Kim, K.-H., Lee, E., Kwon, H.-J., Lee, D.-H., & Jin, H. (2014). Loss of geosynchronous relativistic electrons by EMIC wave scattering under quiet geomagnetic conditions. *Journal of Geophysical Research: Space Physics*, *119*, 8357–8371. https://doi.org/10.1002/2014JA020234

Jordanova, V. K., Farrugia, C. J., Thorne, R. M., Khazanov, G. V., Reeves, G. D., & Thomsen, M. F. (2001). Modeling ring current proton precipitation by electromagnetic ion cyclotron waves during the May 14–16, 1997, storm. *Journal of Geophysical Research*, *106*, 7–22. https://doi.org/10.1029/2000JA002008

Kataoka, R., Asaoka, Y., Torii, S., Terasawa, T., Ozawa, S., Tamura, T., … Mori, M. (2016). Relativistic electron precipitation at international Space Station: Space weather monitoring by Calorimetric Electron Telescope. *Geophysical Research Letters*, *43*, 4119–4125. https://doi.org/10.1002/2016GL068930

Kennel, C. F., & Petschek, H. E. (1966). Limit on stably trapped particle fluxes. *Journal of Geophysical Research*, *71*, 1–28. https://doi.org/10.1029/JZ071i001p00001

Kim, H., Lessard, M. R., Engebretson, M. J., & Lühr, H. (2010). Ducting characteristics of Pc 1 waves at high latitudes on the ground and in space. *Journal of Geophysical Research*, *115*, A09310. https://doi.org/10.1029/2010JA015323

Kubota, Y., Omura, Y., & Summers, D. (2015). Relativistic electron precipitation induced by EMIC-triggered emissions in a dipole magnetosphere. *Journal of Geophysical Research: Space Physics*, *120*, 4384–4399. https://doi.org/10.1002/2015JA021017

Loto'aniu, T. M., Fraser, B. J., & Waters, C. L. (2005). Propagation of electromagnetic ion cyclotron wave energy in the magnetosphere. *Journal of Geophysical Research*, *110*, A07214. https://doi.org/10.1029/2004JA010816

Lysak, R. L., & Song, Y. (2005). Nonlocal interactions between electrons and Alfvén waves on auroral field lines. *Journal of Geophysical Research*, *110*, A10S06. https://doi.org/10.1029/2004JA010803

Marshall, R. A., Nicolls, M., Sanchez, E., Lehtinen, N. G., & Neilson, J. (2014). Diagnostics of an artificial relativistic electron beam interacting with the atmosphere. *Journal of Geophysical Research: Space Physics*, *119*, 8560–8577. https://doi.org/10.1002/2014JA020427

Mende, S., Arnoldy, R., Cahill, L. Jr., Doolittle, J., Armstrong, W., & Fraser-Smith, A. (1980). Correlation between λ4278-Å Optical emissions and a Pc 1 Pearl Event observed at Siple Station, Antarctica. *Journal of Geophysical Research*, *85*, 1194–1202. https://doi.org/10.1029/JA085iA03p01194

Milillo, A., Orsini, S., & Daglis, I. A. (2001). Empirical model of proton fluxes in the equatorial inner magnetosphere: Development. *Journal of Geophysical Research*, *106*, 25,713–25,729. https://doi.org/10.1029/2000JA900158

Miyoshi, Y., Sakaguchi, K., Shiokawa, K., Evans, D., Albert, J., Connors, M., & Jordanova, V. (2008). Precipitation of radiation belt electrons by EMIC waves, observed from ground and space. *Geophysical Research Letters*, *35*, L23101. https://doi.org/10.1029/2008GL035727

Miyoshi, Y. S., Jordanova, V. K., Morioka, A., Thomsen, M. F., Reeves, G. D., Evans, D. S., & Green, J. C. (2006). Observations and modeling of energetic electron dynamics during the October 2001 storm. *Journal of Geophysical Research*, *111*, A11S02. https://doi.org/10.1029/2005JA011351

Nomura, R., Shiokawa, K., Omura, Y., Ebihara, Y., Miyoshi, Y., Sakaguchi, K., … Connors, M. (2016). Pulsating proton aurora caused by rising tone Pc1 waves. *Journal of Geophysical Research: Space Physics*, *121*, 1608–1618. https://doi.org/10.1002/2015JA021681

Omura, Y., & Zhao, Q. (2013). Relativistic electron microbursts due to nonlinear pitch angle scattering by EMIC triggered emissions. *Journal of Geophysical Research: Space Physics*, *118*, 5008–5020. https://doi.org/10.1002/jgra.50477

Ozaki, M., Shiokawa, K., Miyoshi, Y., Kataoka, R., Yagitani, S., Inoue, T., … Jordanova, V. K. (2016). Fast modulations of pulsating proton aurora related to subpacket structures of Pc1 geomagnetic pulsations at subauroral latitudes. *Geophysical Research Letters*, *43*, 7859–7866. https://doi.org/10.1002/2016GL070008

Paulson, K. W., Smith, C. W., Lessard, M. R., Engebretson, M. J., Torbert, R. B., & Kletzing, C. A. (2014). In situ observations of Pc1 pearl pulsations by the Van Allen Probes. *Geophysical Research Letters*, *41*, 1823–1829. https://doi.org/10.1002/2013GL059187

Rasmussen, C. E., Guiter, S. M., & Thomas, S. G. (1993). A two-dimensional model of the plasmasphere: Refilling time constants. *Planetary and Space Science*, *41*(1), 35–43. https://doi.org/10.1016/0032-0633(93)90015-T

Rodger, C. J., Raita, T., Clilverd, M. A., Seppälä, A., Dietrich, S., Thomson, N. R., & Ulich, T. (2008). Observations of relativistic electron precipitation from the radiation belts driven by EMIC waves. *Geophysical Research Letters*, *35*, L16106. https://doi.org/10.1029/2008GL034804

Saito, S., Miyoshi, Y., & Seki, K. (2012). Relativistic electron microbursts associated with whistler chorus rising tone elements: GEMSIS-RBW simulations. *Journal of Geophysical Research*, *117*, A10206. https://doi.org/10.1029/2012JA018020

Sakaguchi, K., Miyoshi, Y., Spanswick, E., Donovan, E., Mann, I. R., Jordanova, V., … Green, J. C. (2012). Visualization of ion cyclotron wave and particle interactions in the inner magnetosphere via THEMIS-ASI observations. *Journal of Geophysical Research*, *117*, A10204. https://doi.org/10.1029/2012JA018180

Sakaguchi, K., Shiokawa, K., Ieda, A., Miyoshi, Y., Otsuka, Y., Ogawa, T., … Rich, F. J. (2007). Simultaneous ground and satellite observations of an isolated proton arc at subauroral latitudes. *Journal of Geophysical Research*, *112*, A04202. https://doi.org/10.1029/2006JA012135

Sakaguchi, K., Shiokawa, K., Miyoshi, Y., Otsuka, Y., Ogawa, T., Asamura, K., & Connors, M. (2008). Simultaneous appearance of isolated auroral arcs and Pc 1 geomagnetic pulsations at subauroral latitudes. *Journal of Geophysical Research*, *113*, A05201. https://doi.org/10.1029/2007JA012888

Samara, M., Michell, R., & Hampton, D. (2012). BG3 glass filter effects on quantifying rapidly pulsating auroral structures. *Advances in Remote Sensing*, *1*(3), 53–57. https://doi.org/10.4236/ars.2012.13005

Semeter, J., Zettergren, M., Diaz, M., & Mende, S. (2008). Wave dispersion and the discrete aurora: New constraints derived from high-speed imagery. *Journal of Geophysical Research*, *113*, A12208. https://doi.org/10.1029/2008JA013122

Shiokawa, K., Nomura, R., Sakaguchi, K., Otsuka, Y., Hamaguchi, Y., Satoh, M., … Connors, M. (2010). The STEL induction magnetometer network for observation of high-frequency geomagnetic pulsations. *Earth, Planets and Space*, *62*(6), 517–524.

Shoji, M., & Omura, Y. (2013). Triggering process of electromagnetic ion cyclotron rising tone emissions in the inner magnetosphere. *Journal of Geophysical Research: Space Physics*, *118*, 5553–5561. https://doi.org/10.1002/jgra.50523

Shoji, M., & Omura, Y. (2014). Spectrum characteristics of electromagnetic ion cyclotron triggered emissions and associated energetic proton dynamics. *Journal of Geophysical Research: Space Physics*, *119*, 3480–3489. https://doi.org/10.1002/2013JA019695

Shoji, M., & Omura, Y. (2017). Nonlinear generation mechanism of EMIC falling tone emissions. *Journal of Geophysical Research: Space Physics*, *122*, 9924–9933. https://doi.org/10.1002/2017JA023883

Stockwell, R. G., Mansinha, L., & Lowe, R. P. (1996). Localization of the complex spectrum: The S transform. *IEEE Transactions on Signal Processing*, *44*(4), 998–1001. https://doi.org/10.1109/78.492555

Thorne, R. M., & Horne, R. B. (1993). Cyclotron absorption of ion-cyclotron waves at the bi-ion frequency. *Geophysical Research Letters*, *20*, 317–320. https://doi.org/10.1029/93GL00089

Tsyganenko, N. A. (2002a). A model of the magnetosphere with a dawn-dusk asymmetry 1. Mathematical structure. *Journal of Geophysical Research*, *107*(A8), 1179. https://doi.org/10.1029/2001JA000219

Tsyganenko, N. A. (2002b). A model of the near magnetosphere with a dawn-dusk asymmetry 2. Parameterization and fitting to observations. *Journal of Geophysical Research*, *107*(A8), 1176. https://doi.org/10.1029/2001JA000220

Usanova, M. E., Drozdov, A., Orlova, K., Mann, I. R., Shprits, Y., Robertson, M. T., … Wygant, J. (2014). Effect of EMIC waves on relativistic and ultrarelativistic electron populations: Ground-based and Van Allen Probes observations. *Geophysical Research Letters*, *41*, 1375–1381. https://doi.org/10.1002/2013GL059024

Usanova, M. E., Mann, I. R., Kale, Z. C., Rae, I. J., Sydora, R. D., Sandanger, M., … Vallières, X. (2010). Conjugate ground and multisatellite observations of compression-related EMIC Pc1 waves and associated proton precipitation. *Journal of Geophysical Research*, *115*, A07208. https://doi.org/10.1029/2009JA014935

Yahnin, A. G., Yahnina, T. A., & Frey, H. U. (2007). Subauroral proton spots visualize the Pc1 source. *Journal of Geophysical Research*, *112*, A10223. https://doi.org/10.1029/2007JA012501